Epigenetic regulation of gingival epithelial cell death induced by short-chain fatty acids

Kazuki Uemichi

Nihon University Graduate School of Dentistry Major in Oral Surgery

(Directors: Prof. Morio Tonogi and Assoc. Prof. Hiromasa Tsuda)

Contents

Abstract

Bacteria in the dental plaque surrounding marginal gingival crevices are thought to cause periodontal disease. Gingival epithelial cells in proximity to mature dental plaque compete nutrients with bacteria in plaques. In addition, dental plaque bacteria produce high concentrations of short-chain fatty acids (SCFAs), such as butyrate and propionate, as bacterial metabolites. Therefore, gingival epithelial cells close proximity to mature dental plaque are at risk of both starvation and exposure to butyrate. In such situation, SCFA-treated gingival epithelial cells undergo cell death. Tsuda and his research group demonstrated that butyrate and propionate induce cell death that is dependent of autophagy and reactive oxygen species (ROSs) generation. However, the precise mechanisms underlying SCFA-induced gingival epithelial cell death is poorly understood. Butyrate is a strong histone deacetylase (HDAC) inhibitor. Therefore, I determined the involvement of HDAC inhibitory activity in SCFA-induced death of gingival epithelial cells. Since it was hard to obtain and maintain primary gingival epithelial cells, a Ca9-22 cell line was used as an *in vitro* counterpart of gingival epithelial cells. Butyrate or propionate-treatment of Ca9-22 cells induced acetylation of histone H3, while pretreatment of the cells with C646, a histone acetyltransferase inhibitor, strongly reduced

the elevated acetylation levels. Accordingly, butyrate or propionate-induced cell death was inhibited by the C646 treatment. Similar results were obtained when other HDAC inhibitors were used. Whole transcriptome analysis revealed that the expression of numerous genes was altered by butyrate-induced histone acetylation. Moreover, some autophagy and ROS-related genes found in the altered genes might induce cell death. These results suggest the need for HDAC-inhibitory activity of bacterial metabolites to induce cell death, and the effects might enhance autophagy and ROS production.

Three-dimensional (3D) cell culture systems are reported to be more physiologically similar to the *in vivo* state than 2-dimensional (2D) models, which are extensively employed in periodontal research. Herein, I developed a 3D gingival tissue model with both epithelial and lamina propria layers using human gingival epithelial Ca9-22 cells and primary gingival fibroblasts. The epithelial layer of the developed 3D gingival tissue culture was treated with butyrate, a metabolite of oral bacteria, and the treatment induced the release of damage-associated molecular patterns, such as DNA and Sin3A associated protein 130 kDa (SAP130). These data suggests that butyrate exposure to the epithelium of 3D gingival epithelial-connective tissue hybrid systems also could induce epithelial cell death and the subsequent release of damage-associated molecular patterns.

Chapter 1

Histone-deacetylase-inhibitory effects of periodontopathic-bacterial metabolites induce human gingival epithelial Ca9-22 cell death

Introduction

Periodontal diseases are thought to be caused by periodontopathic bacteria in the mature dental plaques. Numerous bacteria in the dental plaques produce high concentrations of short-chain fatty acids (SCFAs), such as butyrate and propionate, as metabolic by-products [1], and consume nutrients from the gingival crevicular fluid. Therefore, gingival epithelial cells in proximity to mature dental plaques experience both starvation and exposure to SCFAs. Tsuda et al. have demonstrated that these metabolites not only induce apoptosis but also autophagy-dependent death of the human gingival epithelial cells in nutrient insufficient condition and subsequent release of high mobility group box 1 (HMGB1), which activates innate immunity when released into the extracellular spaces [2-4]. Thus, cell death induced by SCFAs is important for understanding periodontal disease initiation.

Histone acetylation status is involved in the epigenetic regulation of gene expression (Fig. 1) [5]. The *N*-terminals of the histone proteins have several lysine residues that can be acetylated by histone acetyltransferases (HATs). In addition, histone deacetylases (HDACs) remove acetyl groups from the acetylated sites (Fig. 1). As lysine residues of non-acetylated histones exhibit cationic characteristics in the nucleus, negatively charged DNA is strongly associated with histones (closed chromatin). Thus, transcriptional

machinery cannot bind to the promoter and/or enhancer regions of the chromosomes, resulting in a transcriptionally inactive state. In contrast, acetylation of the histone lysine residues leads to a transcriptionally active state, in which transcriptional machinery can easily access promoter and/or enhancer regions. Acetylation of the lysine residues results in the clearance of their positive charge, and the affinities of the histone proteins to the DNA is attenuated.

Although the involvement of autophagy and reactive oxygen species (ROSs) in the death of gingival epithelial cells has been reported [2-4], the precise induction mechanisms of the death of gingival epithelial cells through butyrate treatment are still unclear. As butyrate is known to have an HDAC-inhibitory character [6], I focused on the epigenetic regulation of gene transcriptions, especially on those with histone acetylation. HDAC inhibition leads to enhanced acetylation of histones and further activation of gene transcriptions [5]. In this study, I evaluated the involvement of HDAC-inhibitory activities of metabolites produced by periodontopathic bacteria in the death of gingival epithelial cells and further discussed the mechanisms of SCFA-induced gingival cell death.

Materials and methods

Antibodies. Horseradish peroxidase (HRP)-conjugated anti-acetyl-histone H3 (Lys9) rabbit monoclonal antibody and HRP-conjugated anti-human glycelaldehyde-3-phosphate dehydrogenase (GAPDH) rabbit polyclonal antibody were purchased from Cell Signaling Technologies (Danvers, MA, USA) and Wako (Osaka, Japan), respectively.

Media and reagents. Minimum essential medium α (MEMα), Roswell Park Memorial Institute (RPMI) 1640 media, sodium butyrate, and sodium propionate were purchased from Wako. Fetal bovine serum (FBS) was purchased from Biofill Australia (Victoria, Australia). Valproic and suberoylanilide hydroxamic acids (SAHA) were obtained from Cayman Chemical (Ann Arbor, MI, USA). C646 (AdipoGen Life Sciences, Liestal, Switzerland) was diluted in dimethylsulfoxide (DMSO, Wako) to constitute a stock solution.

Cell cultures. Human gingival Ca9-22 cells (Riken BioResource Research Center, Tsukuba, Japan), which are often used as counterparts of human gingival epithelial cells [7-10], were maintained in 10% FBS MEMα supplemented with 1% penicillin/streptomycin (Wako) at 37℃ in a 5% CO_2 atmospheric condition.

Western blot. Ca9-22 cells were seeded in 12-well plates (4×10^5 cells/well) and incubated overnight at 37°C. The cells were then treated for 6 h with 1% FBS RPM1640

containing each HDAC inhibitor (5 mM sodium butyrate, 10 mM sodium propionate, 5 mM valproic acid, or 10 μM SAHA). For the HAT inhibition, cells were pretreated for 1 h with C646 in 10% FBS MEMα before treatment with HDAC inhibitors. After treatment, cells were lysed in Laemmli sample buffer and sonicated. Aliquots of the same volume of lysates were subjected to sodium dodecyl sulfate-polyacrylamide gel electrophoresis (5%-20% polyacrylamide gradient gel). The electrophoresed proteins were transferred onto a polyvinylidene difluoride membrane (Wako). The membrane was treated with an Ez-Block Chemi blocking reagent (ATTO, Tokyo, Japan) for 30 min and then with HRP-conjugated anti-acetyl histone H3 or GAPDH antibodies for 1 h. After serial washing with Tris-buffered saline containing 0.1% Tween 20, the band images were developed using a Clarity Western ECL reagent (Bio-Rad Laboratories, Hercules, CA, USA) and photographed using ChemiDoc XRS system (Bio-Rad Laboratories).

SYTOX-Green dye cell death assay. The necrotic dead cell count was measured as described in previous reports [2,3]. Briefly, Ca9-22 cells (3×10^4 cells/well) in a 96-well black plate with a transparent bottom were pretreated for 1 h with several concentrations of C646 (0, 6.25, 12.5, or 25 μM) in 10% FBS MEMα. Thereafter, the cells were treated for 48 h with 100 μL of 1% FBS RPMI1640 (Wako) containing sodium butyrate, sodium propionate, valproic acid, or SAHA in the presence of the same serial concentrations of

C646. Next, 100 μL of 400 nM SYTOX-Green dye (Thermo Fisher Scientific, Waltham, MA, USA) in phenol-red free RPMI1640 was added to each well and the emitted fluorescence intensity (Ex/Em = 485/535 nm), which reflects the number of dead cells, was measured using a Wallac ArvoSX1420 spectrofluorometer (PerkinElmer, Waltham, MA, USA). An equal volume of phenol-red free RPMI1640 was added instead of SYTOX-Green dye solution for background establishment.

Visualization of SYTOX-green stained cells. Ca9-22 cells (1.6×10^5 cells) in wells of 24-well plates were pretreated for 1 h with several concentrations of 25 μM C646. Subsequently, the cells were treated for 48 h with 5 mM butyrate, 10 mM propionate, 10 μM SAHA, or 5 mM valproic acid in the presence or absence of 25 μM C646. Thereafter, SYTOX-green dye (1 : 12500 diluted in phenol-red free RPMI1640) was added, and green fluorescence images were visualized by Keyence BZ-X810 (Keyence, Osaka, Japan).

RNA-sequencing analysis. Ca9-22 cells (1×10^6 cells/well) were seeded in a 6-well plate and incubated overnight at 37°C. The medium was changed to 10% FBS MEMα, and the cells were preincubated for 1 h. The cultures were then treated for 6 h or left untreated with 5 mM sodium butyrate in 1% FBS RPMI1640. For the HAT inhibition, the cells were pretreated for 1 h with 25 μM C646 and then treated for 6 h with 5 mM sodium butyrate

in the presence of 25 μM C646. Total RNA was extracted and purified using ISOGEN with a Spin Column Kit (NIPPON GENE, Tokyo, Japan). RNA concentrations and qualities were checked using NanoDrop (Thermo Fisher) and Bioanalyzer (Agilent Technologies, Santa Clara, CA, USA) devices. For RNA-sequencing analysis, RNA libraries were prepared using the NEBNext Ultra RNA Library Prep Kit for Illumina (NEB, Ipswich, MA, USA). Paired-end sequencing was performed (150 × 2 bp, 40 M reads, and 6 GB data/sample) using a Novaseq next-generation sequence system (Illumina, San Diego, CA, USA). Sequence quality was checked using FastQC software (ver.0.11.7, Babraham Institute, Cambridge, UK), and sequence trimming and mapping of read sequences were performed using Trimmomatic (ver.0.38, The USADEL LAB, Aachen, Germany) and HISAT2 (ver. 2.1.0, The University of Texas Southwestern Medical Center, Dallas, TX, USA) software, respectively. Read counts and transcripts per million (TPM) calculations were performed using FeatureCounts software (ver.1.6.3, Olivia Newton-John Cancer Research Institute Melbourne, Australia). The cut-off value for TPM was < 0.01. For gene ontology (GO) enrichment analysis, Metascape gene annotation and analysis resources (https://metascape.org/gp/index.html#/main/step1) [11] were used. Logalisms of each gene TPM to the base 2 were calculated and plotted as a scatter plot. Mean ratio (M) and average (A) of logalisms of each gene TPM to the base 2 were

calculated and plotted as a MA plot. The number of genes which were upregulated by butyrate treatment more than twice and those which were reduced in the presence of C646 less than a half were calculated. The calculation and Venn diagram drawing were performed using Microsoft Excel software (Microsoft, Redmond, WA). Transcriptome data that are demonstrated in this study are openly available in the DNA Data Bank of Japan (Mishima, Japan) at http://www.ddbj.nig.ac.jp/, accession number DRA014468.

Statistical analysis. All statistical analyses in this study were performed using EZR (Saitama Medical Center and Jichi Medical University, Saitama Japan) [12], which is a graphical user interface for R (The R Foundation for Statistical Computing, Vienna, Austria). Precisely, it is a modified version of the R commander designed to add statistical functions frequently used in biostatistics. Since the data were not normally distributed (the Shapiro-Wilk test was conducted), Kruskal−Wallis test followed by the Steel test was used to examine the differences. p-values < 0.05 was considered statistically significant.

Results

Butyrate or propionate treatment induces increase of histone H3 acetylation in human gingival epithelial Ca9-22 cells, and C646 reduced the increase. To investigate whether butyrate and propionate act as HDAC inhibitors, the acetylation levels of histone H3 after butyrate or propionate treatment of human gingival Ca9-22 cells were determined. As shown in Figure 2A, increased acetylation levels of histone H3 were observed in butyrate and propionate-treated Ca9-22 cells than those in the control cells. As HAT activity was not inhibited, HDAC inhibition induced the increased acetylation level of histone H3. Next, the effect of HAT inhibition on histone H3 acetylation levels was examined using C646, a specific inhibitor of p300 histone acetyltransferase. C646-pretreatment strongly reduced the butyrate or propionate-induced increase of histone H3 acetylation (Fig. 2B).

Decreased acetylation levels of histone by HAT-inhibition attenuate butyrate or propionate-induced Ca9-22 cell death. To examine whether the decrease in histone acetylation affects butyrate or propionate-induced Ca9-22 cell death, p300 histone acetyltransferase was inhibited by C646 pretreatment, and the induction of cell death was measured. C646 pretreatment reduced both butyrate and propionate-induced Ca9-22 cell death (Fig. 3A, B). The fluorescence images corresponded to the data obtained from the

SYTOX-green dye cell death assay (Fig. 3C).

Treatment with other HDAC inhibitors induces Ca9-22 cellular death. To examine whether HDAC inhibition induces Ca9-22 cell death, the effects of valproic acid and SAHA, which are often used as HDAC inhibitors, were also tested in the cells. Treatment of Ca9-22 cells with both valproic acid and SAHA increased histone H3 acetylation levels and the number of dead cells in a dose-dependent manner (Fig. 4A-D).

HAT inhibition reduces valproic acid or SAHA-induced Ca9-22 cell death. To examine whether valproic acid and SAHA-induced Ca9-22 cell death is related to histone acetylation, the effects of HAT inhibition by C646 on histone acetylation levels and cell death induced by valproic acid and SAHA were examined. As shown in Figure 5A and B, C646 reduced the valproic acid and SAHA-induced increased acetylation levels of histone H3 in a dose-dependent manner, with strong suppression at a C646 concentration of 25 μM. In addition, C646 treatment resulted in a dose-dependent reduction of Ca9-22 cell death following valproic acid or SAHA treatment (Fig. 5C, D). Fluorescence images were correspondent with the data obtained from the cell death assay (Fig. 5E).

A transcriptome analysis. As described above, treatment of Ca9-22 cells with HDAC inhibitors induced increase of histone acetylation, and the increase was required for cell death. In addition, the acetylation of histone tails was thought to result in transcriptional

activation. Therefore, I examined the effects of butyrate treatment (on behalf of treatment of HDAC inhibitors) on whole transcript expressions using high throughput sequencing technology to extract candidate genes related to cell death mechanisms induced by butyrate treatment. Butyrate-treatment upregulated 4175 genes with expression levels more than twice that of the control treatment (Fig. 6A, B, and Table 1). In addition, butyrate treatment also reduced the expression of 3196 transcripts, which was less than half that of the control treatment (Fig. 6A, B, and Table 1). Since acetylation of histone tails is thought to result in gene upregulation and translated proteins can affect phenotypic changes, I next focused on the upregulated protein-coding genes by butyrate-induced histone acetylation. Butyrate treatment induced the upregulation of 2453 protein-coding genes which were expressed more than twice that of the control (Fig. 6C). HAT inhibition by C646 treatment reduced the expression of 979 genes, which were less than half of that in butyrate-treated cells, among these, 749 genes were upregulated by butyrate treatment more than twice that of the control treatment (Fig. 6C). Among these 749 genes, the top 20 protein-coding genes are listed according to the induction level by butyrate treatment in Table 2. Since these 749 transcripts may contain candidate transcripts related to the mechanisms of butyrate-induced cell death, gene ontology (GO) enrichment analysis was performed using the candidate gene list (of which only 735 genes which have Entrez Gene

ID were used for enrichment). Genes related to autophagy or ROS were selected from the results of GO enrichment analysis. Table 3 lists 17 or 11 genes that were enriched by the keywords autophagy or ROS, respectively. *IRGM*, *ATG4B*, and *ATG2A* were found in the list of autophagy-related genes, and *NOX5* in that of ROS-related genes (Table 3). Acetylation of histones results in transcriptionally active status (Fig. 1) [5]. Therefore, putative transcription-factor binding sites were examined using transcription factor target GOs. Every putative transcription factor binding site is named according to the corresponding GO numbers. Each GO number is annotated to the genes which have GO sites in 4-kbp upstream or downstream of the transcription start sites. The top 20 GOs (transcription factor target sites), which were found around the genes upregulated by histone acetylation, are listed in Table 4. In addition, autophagy and ROS-related genes which has been linked to corresponding GOs were listed in Table 4.

Discussion

Butyrate and propionate can induce human gingival epithelial cell death in serum-decreased conditions [2-4]. In this study, I confirmed that butyrate and propionate possess HDAC-inhibitory characteristics. Since both SCFAs increased histone H3 acetylation but they did not induce increase of histone H3 acetylation when HAT was inhibited (Fig. 1A and B), they are thought to function as HDAC inhibitors. In addition, HAT inhibition reduced butyrate or propionate-induced gingival epithelial cell death (Fig. 3). These findings suggest that the HDAC inhibitory activities of butyrate and propionate are important for SCFA-induced death of gingival epithelial cells. Additionally, valproic acid and SAHA, which are well-known HDAC inhibitors, also induced Ca9-22 cell death, and these phenotypes were almost completely inhibited by HAT inhibition (Figs. 4 and 5). These data support the importance of HDAC inhibitory activity in cell death.

As shown in Figure 1, the acetylation of histones epigenetically controls gene expression. Since the conditions that induce cell death are accompanied by strong histone acetylation (Figs. 2-5), some genes upregulated by HDAC inhibitor treatments may include notable genes related to cell death mechanisms. Therefore, 749 genes upregulated by butyrate treatment and downregulated by C646 pretreatment in the presence of butyrate were investigated (Fig. 6C). Among these 749 genes (735 genes which have

Entrez gene ID were selected from 749 protein-coding genes), 17 and 11 genes were related to autophagy and ROS, respectively (Table 3). The most induced autophagy related gene by butyrate treatment was *IRGM* (Table 2). This gene was ranked second among 749 genes (Table 2). *IRGM* has been reported to induce autophagy by facilitating the co-assembly of *ULK1* and *BECLIN1* gene products, and this complex allows the progression of autophagy [13]. In addition, upregulation of *ATG4B* and *ATG2A* genes, which are important for LC3B anchoring on autophagosomes and autophagosome assembly [14,15], respectively, were also found in the autophagy-related gene list (Table 3). Therefore, butyrate-induced increase of histone acetylation might be related to autophagy induction. In contrast, *NOX5*, which codes for an NADPH oxidase [16], was ranked first in the ROS-related genes. In addition, many autophagy or ROS-related genes were found in putatively controlled genes by enriched transcription factor binding site (Table 4). Since previous reports have demonstrated that butyrate-induced death of Ca9-22 cells requires autophagy and ROS [4,17], elevated histone acetylation level may induce autophagy and ROS production, thereby leading to cell death. Further investigation for relationships between autophagy, ROS, and increased histone acetylation induced by SCFA treatment is needed to understand the HDAC inhibitor-induced cell death better.

In mature dental plaque, numerous live bacteria consume a huge amount of nutrients. Therefore, gingival epithelial cells facing to mature dental plaques are at nutrient insufficiency risk in addition to SCFA exposure. Nutrient depletion activates adenosine monophosphate-activated protein kinase (AMPK), and the activation of the kinase induces autophagy [18]. Evans et al. have previously demonstrated that gingival epithelial cells incubated in the presence of low FBS condition (1% FBS) activated AMPK and subsequently induced autophagy [3]. However, this condition triggered only a small number of dead cells [3], indicating that the autophagy levels in the absence of butyrate are insufficient to induce cell death and that butyrate treatment provides sufficient autophagy-related gene products. In addition, ROS have been reported to induce autophagy [19]. Therefore, both nutrient-insufficient condition and exposure to SCFAs, which has HDAC-inhibitory character, may induce much stronger autophagy upregulation than that in non-HDAC inhibitor condition, and results in SCFA-induced cell death.

Tsuda and his collegues demonstrated that butyrate treatment with gingival epithelial cells induces cellular death, and that the cell death induction requires upregulation of autophagy [2,3], AMPK activation [3], and ROS generation [4]. In the present study, I have demonstrated that inhibition of HDAC also required for butyrate-and propionate-

induced gingival epithelial cell death. This is a novel finding from this study. Ebe et al. had demonstrated earlier using the Ca9-22 gingival epithelial cell line that butyrate-treated cells showed a slightly swollen and necrotic morphology accompanied by broken cellular membranes [17]. In addition, Liu et al. demonstrated using primary human gingival epithelial cells that cell death induced by butyrate treatment is gasdermin-E-dependent pyroptosis, which accompanies swelling and bubble morphology of dead cells [20]. However, neither report referred to the effects of HDAC inhibition on the induction of SCFA-induced cell death. Further studies are warranted to elucidate the effects of butyrate and propionate on HDAC activity and associated cell death. I plan to explore this aspect in my future studies.

Dental plaque bacteria accumulate around the marginal gingiva, causing gingival symptoms, such as redness and swelling of gingiva. This suggests that bacterial accumulation causes gingival inflammation. Dental plaque composed of numerous live bacteria, consume large amounts of nutrients. Therefore, gingival epithelial cells in contact with mature dental plaque compete for nutrients with the plaque bacteria. Under the nutrient depleted conditions, bacteria in mature plaques produce high concentrations of SCFAs, such as butyrate and propionate [1]. Fujiwara et al. demonstrated that this condition induces death of gingival epithelial cells and there is subsequent release of

damage-associated molecular patterns (DAMPs), such as HMGB1 [4]. Extracellular release of the molecule reportedly induce neutrophil migration [21] and inflammatory cytokine production [22]. Therefore, SCFA-induced gingival cell death that I have observed may be important for the onset of gingivitis. In this study, my data suggests that the HDAC-inhibitory activity of periodontopathic bacterial metabolites is important for inducing human gingival epithelial Ca9-22 cell death. In addition, I demonstrated that treatment of Ca9-22 cells with HAT inhibitors, such as C646, decreased histone acetylation and cell death. Therefore, treatment of gingival epithelial tissue with HAT inhibitors might be useful for the prevention of gingivitis. However, the experimental system that I used was a two-dimensional culture system that used a gingival epithelial cell line. Three-dimensional culture systems allow cells to interact more easily with their surroundings in all directions compared to two-dimensional models. Hence, three-dimensional culture systems using primary cells are thought to be most analogous to real tissues [23]. This is the current limitation of my experimental study. Thus, confirmation of these phenomena using a three-dimensional system with primary gingival epithelial cells is needed.

Table 1. The number of the up or down-regulated transcripts by butyrate treatment.

type of transcripts	the number of transcripts
Upregulated transcripts (log2(Buty/Cont) ≧ 1)	**4175**
protein coding	2453
miRNA	3
lincRNA	426
antisense	561
others	722
Downregulated trasncripts (log2(Buty/Cont) ≦ -1)	**3196**
protein coding	1701
miRNA	18
lincRNA	415
antisense	466
others	596

Table 2. Butyrate-upregulated protein-coding genes which were suppressed by C646 treatment.

ranking	gene symbol	log_2(Buty)-log_2(Cont)	log_2(Buty+C646)-log_2(Buty)
1	*COL26A1*	7.365	-5.162
2	*IRGM*	7.086	-6.583
3	*AC093323.1*	7.040	-5.644
4	*FAM153A*	6.950	-4.126
5	*CCR4*	6.930	-6.428
6	*TM4SF18*	6.817	-4.314
7	*RGMA*	6.707	-5.439
8	*PKNOX2*	6.699	-6.813
9	*NECTIN3*	6.290	-2.202
10	*GBP5*	6.007	-5.642
11	*PCP4L1*	5.960	-3.457
12	*ZDHHC19*	5.940	-2.438
13	*RADIL*	5.936	-2.801
14	*CYP4F2*	5.798	-4.074
15	*ENPP2*	5.673	-1.756
16	*BRS3*	5.633	-2.961
17	*NR1H4*	5.608	-1.106
18	*ZBTB8B*	5.478	-1.516
19	*U2AF1L5*	5.428	-4.684
20	*COL20A1*	5.369	-3.867

Table 3. Genes in Autophagy or ROS-related GO terms enriched using metascape.

gene symbol	log_2(Buty)-log_2(Cont)	log_2(Buty+C646)-log_2(Buty)
autophagy-related genes		
IRGM	7.086	-6.583
NPC1	3.287	-2.913
MAPK15	2.998	-1.911
SYNPO2	2.791	-1.902
MAPT	2.676	-2.911
NLRP6	2.666	-1.922
RMC1	2.424	-1.404
MCOLN1	1.978	-1.557
WIPI1	1.844	-1.734
ATG4B	1.692	-1.251
LAMP3	1.566	-1.631
ACER2	1.386	-1.093
ATG2A	1.266	-1.557
SPATA33	1.245	-1.167
SLC25A4	1.220	-1.123
ZFYVE1	1.134	-1.564
ATP6V1D	1.038	-1.686
ROS-related genes		
NOX5	4.505	-3.003
ABCD2	2.920	-1.570
CYP2E1	2.884	-1.382
MAPT	2.676	-2.911
GPR37	2.423	-2.013
TPO	2.394	-2.892
TXNIP	1.644	-2.979
UCP2	1.413	-1.589
MAOB	1.303	-1.122
SMPD3	1.257	-1.562
GNAI2	1.157	-1.053

Table 4. Top 20 transcription-factor target-site GOs which were upregulated by histone acetylation.

Rank	transcription-factor target-site GOs	# of genes with GO sequence in the hit genes	% in the hit genes	Genes with GO sequences listed in Table 3	
				Genes related to autophagy	Genes related to ROS
1	M13849	36	4.9	*WIPI1*	*SMPD3*
2	M9769	36	4.9	*MAPT*	*ABCD2*, *MAPT*
3	M11439	29	3.9	*ATG4B*, *ZFYVE1*, *MAPT*	*SMPD3*, *MAPT*
4	M4815	28	3.8	*SLC25A4*	*ABCD2*
5	M1607	27	3.7		*MAOB*
6	M15558	26	3.5		
7	M2211	26	3.5	*WIPI1*	
8	M12520	25	3.4	*MAPK15*	
9	M40788	24	3.3		*NOX5*
10	M15101	22	3.0	*ZFYVE1*	
11	M17420	22	3.0	*WIPI1*	
12	M6628	21	2.9		
13	M2120	19	2.6		*MAOB*
14	M1460	19	2.6		
15	M6446	18	2.4	*MAPT*	*GNAI2*, *MAPT*
16	M9024	17	2.3		
17	M2209	17	2.3	*ZFYVE1*	*GNAI2*
18	M19265	17	2.3	*ZFYVE1*	
19	M8059	17	2.3		
20	M16022	17	2.3	*SLC25A4*, *WIPI1*	*CYP2E1*

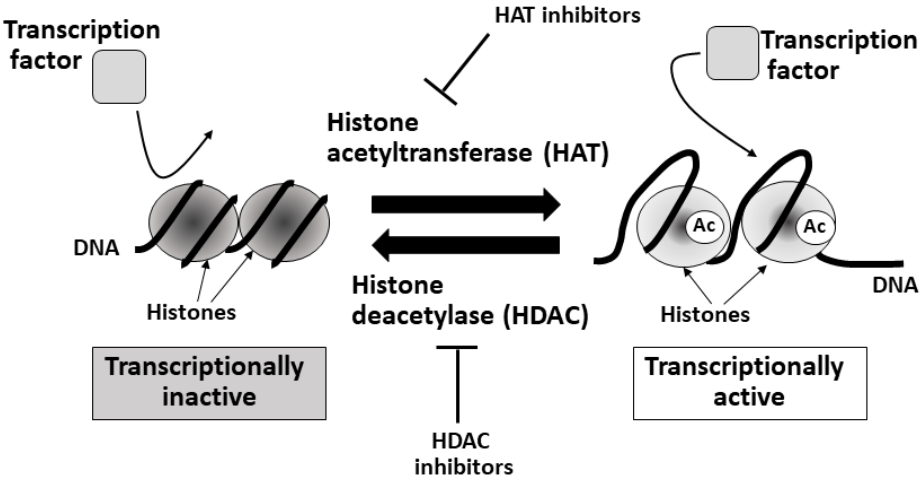

Fig. 1 A schematic illustration of the relationship between the histone-acetylation state and its modulators. HATs acetylate histone tails, and HDACs remove acetyl groups from acetylated histones. Increase of histone acetylation is induced when HDACs are suppressed by their inhibitors, such as sodium butyrate. In contrast, histone acetylation is decreased when cells are treated with HAT inhibitors, such as C646. Since ionized lysine residues of histone tails and DNA exhibit positive and negative charges, respectively, histones are tightly wrapped by DNAs. Therefore, transcription factors cannot bind their promoters or enhancer/silencer motifs on DNA, resulting in a transcriptionally inactive state. In contrast, acetylation of lysine residues of amine groups reduces the affinities between histone tails and DNA. This causes DNA to unwind from histones, resulting in a transcriptionally active state. HAT, histone acetyltransferase; HDAC, histone deacetylase.

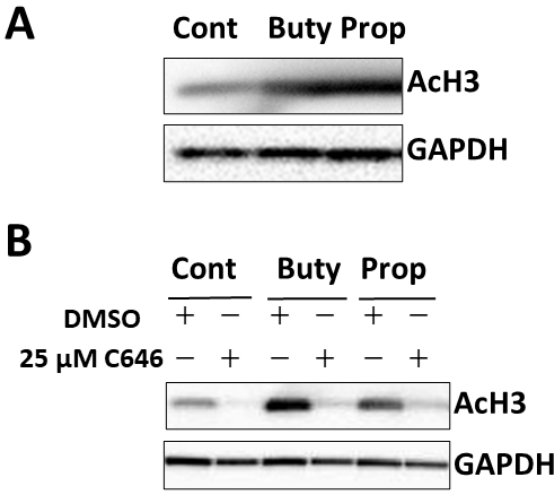

Fig. 2 Treatment of Ca9-22 cells with sodium butyrate or sodium propionate induced histone H3 acetylation, while HAT inhibition by C646 reduced the effects. (A) Ca9-22 cells were treated for 6 h with 5 mM sodium butyrate or 10 mM sodium propionate, and cell lysates were subjected to western blotting. (B) Ca9-22 cells were pretreated with 25 μM C646 or DMSO (for vehicle control) for 1 h and subsequently treated for 6 h with 5 mM sodium butyrate or 10 mM sodium propionate in the presence of C646. Cellular lysates were subjected to western blotting. Cont, control treatment; Buty, butyrate treatment; Prop, Propionate treatment; AcH3, acetylated histone H3; GAPDH, glyceraldehyde-3-phosphate dehydrogenase.

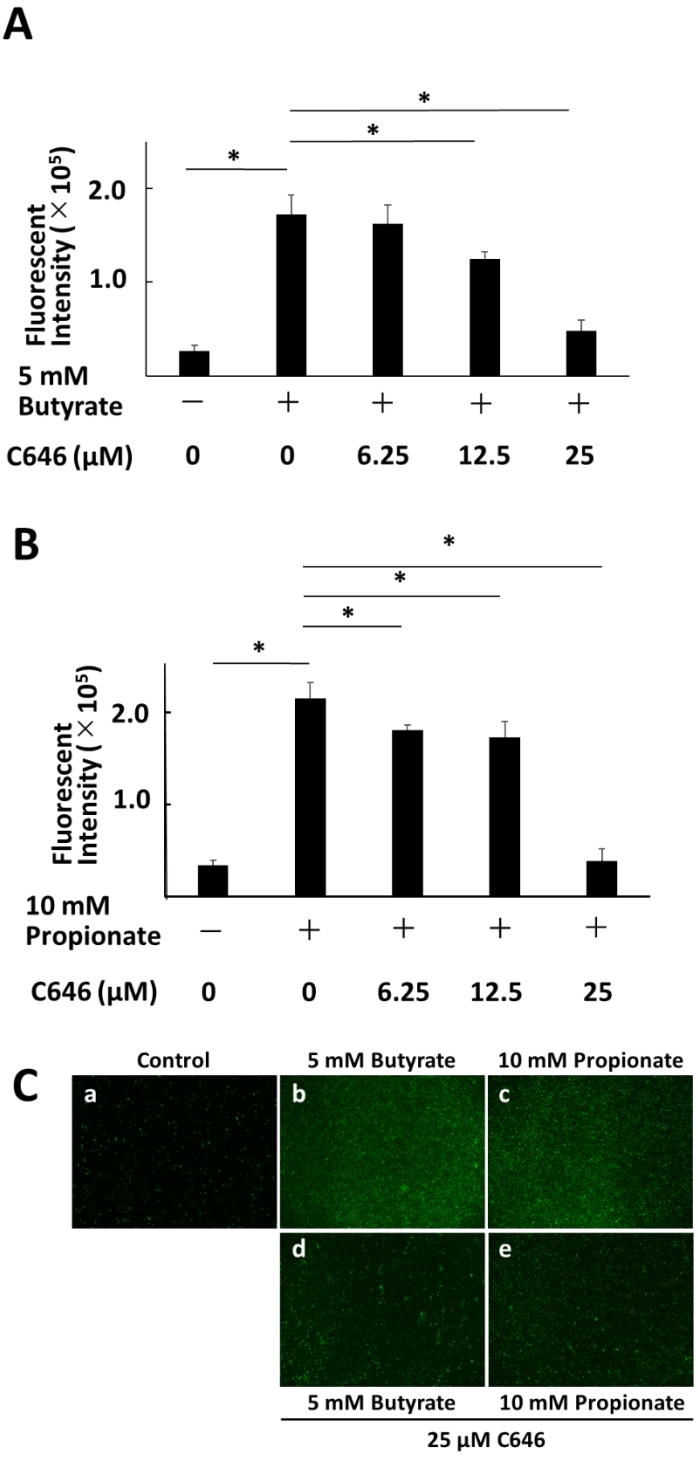
A
Fluorescent Intensity (×10⁵)
2.0
1.0
*
*
*
5 mM Butyrate
− + + + +
C646 (μM) 0 0 6.25 12.5 25
B
Fluorescent Intensity (×10⁵)
2.0
1.0
*
*
*
*
10 mM Propionate
− + + + +
C646 (μM) 0 0 6.25 12.5 25
C
Control
5 mM Butyrate
10 mM Propionate
a
b
c
d
e
5 mM Butyrate
10 mM Propionate
25 μM C646

Fig. 3 HAT inhibition by C646 reduced butyrate or propionate-induced Ca9-22 cell death in a dose-dependent manner. Ca9-22 cells were pretreated for 1 h with the indicated concentrations of C646 and then treated for 48 h with 5 mM sodium butyrate (A) or 10 mM sodium propionate (B) in the presence of the same concentration of C646. The dead cell counts were measured using fluorescence intensities of SYTOX-green dye (n = 8; *, $p < 0.01$). (C) Ca9-22 cells pretreated for 1 h with or without 25 μM C646 and subsequently treated for 48 h with 5 mM butyrate (panels b and d), 10 mM propionate (panels c and e) in the presence (panels d and e) or absence (panels a, b, and c) of 25 μM C646. After addition of SYTOX-green dye, green fluorescence images were visualized.

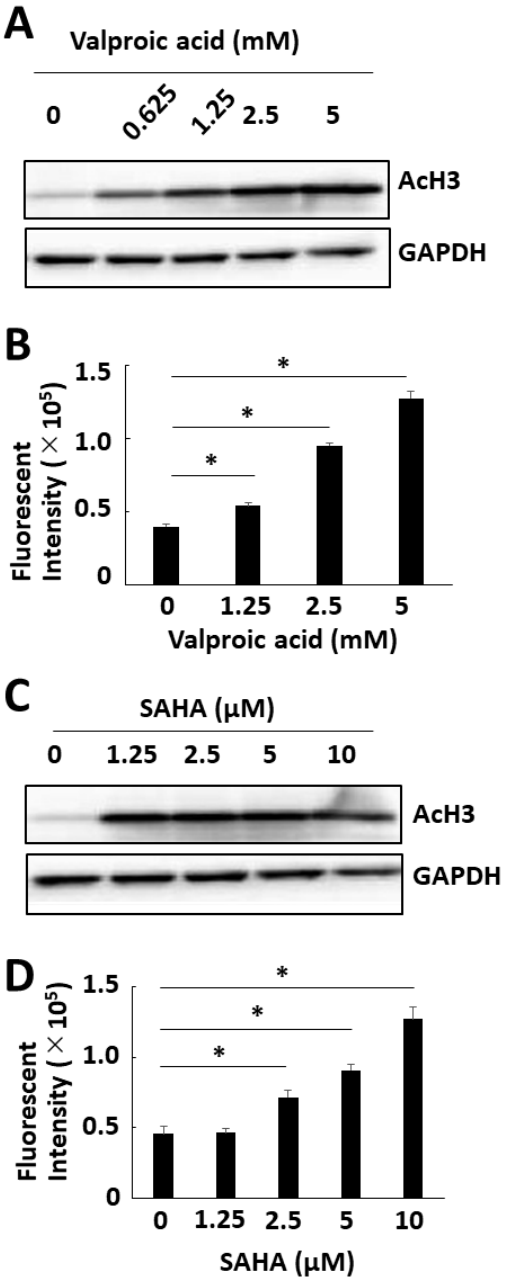

Fig. 4 Valproic acid and SAHA induced histone H3 acetylation and Ca9-22 cell death. (A and C) Ca9-22 cells were treated for 6 h with the indicated concentrations of valproic acid or SAHA, and cell lysates were subjected to western blotting. (B and D) Ca9-22 cells were treated for 48 h with the indicated concentrations of valproic acid or SAHA, and the dead cell counts were measured using fluorescence intensities of SYTOX-green dye (n = 8; *, $p < 0.01$).

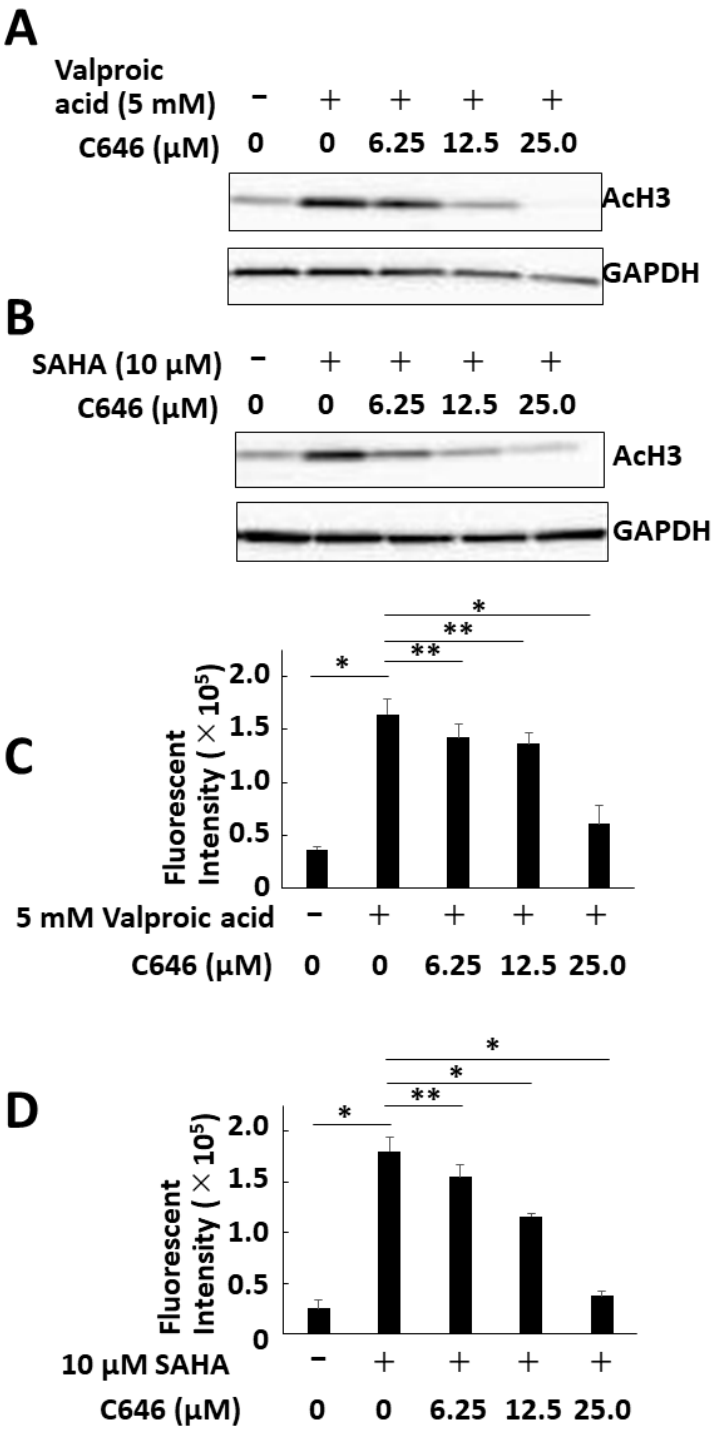
A
Valproic acid (5 mM) - + + + +
C646 (μM) 0 0 6.25 12.5 25.0
AcH3
GAPDH
B
SAHA (10 μM) - + + + +
C646 (μM) 0 0 6.25 12.5 25.0
AcH3
GAPDH
C
Fluorescent Intensity (×10⁵)
2.0
1.5
1.0
0.5
0
*
**
**
*
5 mM Valproic acid - + + + +
C646 (μM) 0 0 6.25 12.5 25.0
D
Fluorescent Intensity (×10⁵)
2.0
1.5
1.0
0.5
0
*
**
*
*
10 μM SAHA - + + + +
C646 (μM) 0 0 6.25 12.5 25.0

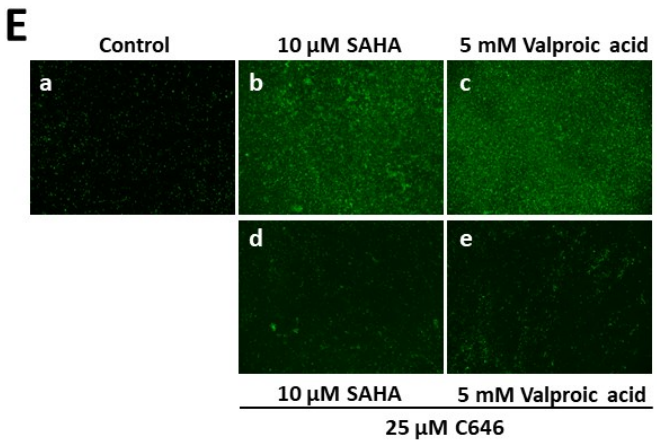

Fig. 5 C646 reduced valproic acid or SAHA-induced histone H3 acetylation in a dose-dependent manner. (A and B) Ca9-22 cells were pretreated for 1 h with the indicated concentrations of C646 and subsequently treated for 6 h with 5 mM valproic acid (A) or 10 μM SAHA (B) in the presence of the same concentrations of C646. Cell lysates were subjected to western blotting. (C and D) Ca9-22 cells were pretreated for 1 h with the indicated concentrations of C646 and subsequently treated for 48 h with 5 mM valproic acid (C) or 10 μM SAHA (D) in the presence of the same concentrations of C646. The dead cell counts were measured using fluorescent intensities of SYTOX-green dye (n = 8; *, $p < 0.01$; **, $p < 0.05$). SAHA, suberoylanilide hydroxamic acid. (E) Ca9-22 cells pretreated for 1 h with or without 25 μM C646 and then treated for 48 h with 10 μM SAHA (panels b and d), and 5 mM valproic acid (panels c and e) in the presence (panels d and e) or absence (panels a, b, and c) of 25 μM C646. Green fluorescence images were visualized after the addition of SYTOX green dye.

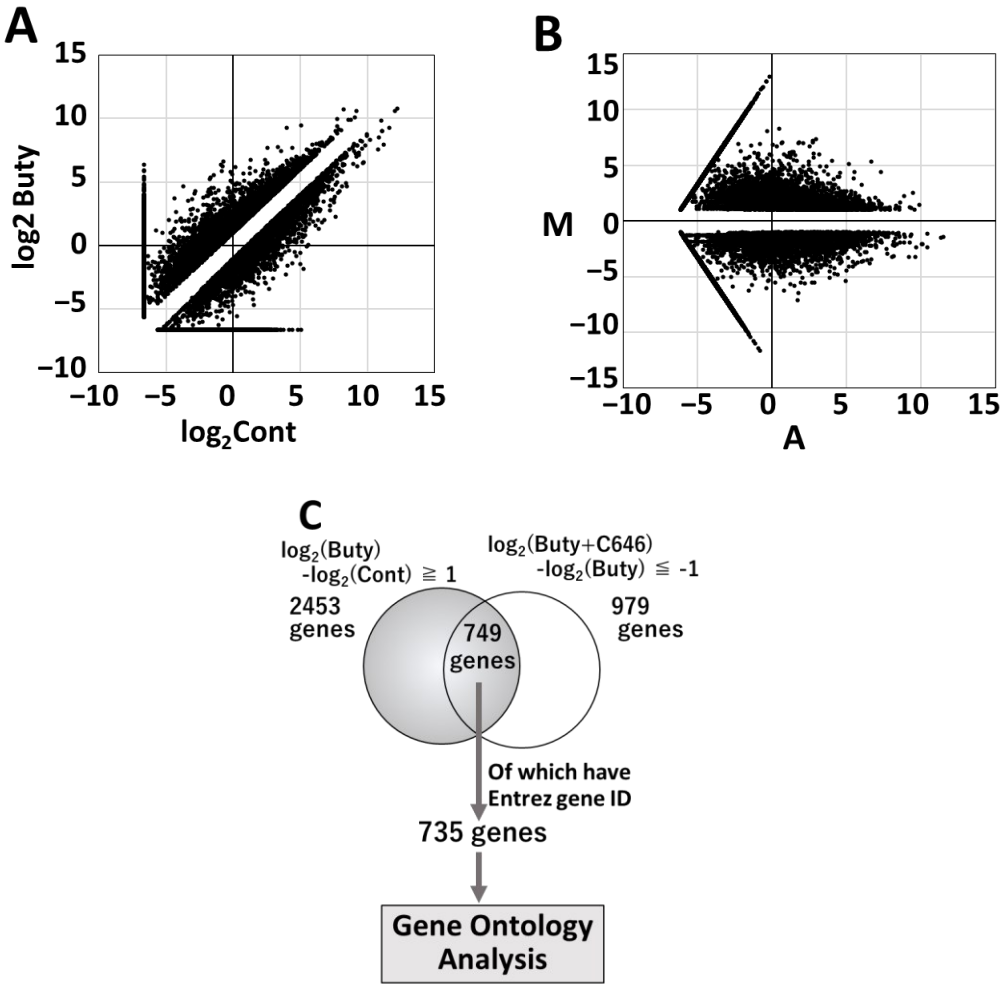

Fig. 6 RNA sequencing analysis. Ca9-22 cells were treated for 6 h with (Buty) or without (Cont) 5 mM sodium butyrate. For HAT inhibition, cells were pretreated for 1 h with 25 μM C646. Total RNA was extracted from the cells, and RNA sequences were analyzed. (A and B) TPM < 0.01 were omitted, and the scatter (A) and the M-A (B) plots of Buty and Cont were plotted. (C) A Venn diagram showing 749 butyrate-upregulated genes, which were downregulated by butyrate treatment in the presence of C646. For GO enrichment analysis, 735 genes which have Entrez gene ID were used. Buty, butyrate treatment. Cont, control treatment. Buty+C646, butyrate treatment in the presence of C646.

Chapter 2

Butyrate-treatment induces gingival epithelial cell death in a three-dimensional gingival-connective tissue hybrid co-culture system

Introduction

Two-dimensional (2D) culture systems have long been employed to examine the pathogenic mechanisms associated with periodontal diseases. Despite numerous reports using conventional 2D culture systems, the molecular mechanisms underlying periodontal disease remain elusive. Recent advances in cell culture techniques have enabled the development of three-dimensional (3D) culture systems, potentially allowing cells to mimic the *in vivo* environment more accurately [23]. For developing 3D gingival culture systems, it is desirable to use primary gingival epithelial cells and fibroblasts. However, obtaining primary gingival epithelial cells that lack fibroblast contamination can be challenging. Therefore, I developed a gingival 3D culture model consisting human gingival epithelial Ca9-22 cells and primary gingival fibroblasts.

Following the development of mature dental plaque, bacteria produce high concentrations of short-chain fatty acids (SCFAs), such as butyrate [1]. In a previous study using a 2D culture system, treatment of gingival epithelial cells with butyrate was shown to induce cellular death, accompanied by the release of intracellular molecules called damage-associated molecular patterns (DAMPs), which can induce the production of proinflammatory cytokines [3,4]. Herein, I developed a gingival 3D culture system and examined the effects of butyrate on gingival layers.

Materials and methods

Antibodies. An anti-human cytokeratin mouse monoclonal antibody (clone AE1/AE3), an anti-human vimentin mouse monoclonal antibody (clone V9), an anti-Sin3A associated protein 130 kDa (SAP130) rabbit polyclonal antibody, and a WestVision secondary antibody labeled with horseradish peroxidase were purchased from DAKO (Glostrup, Denmark), Leica-Novocastra (Newcastle upon Tyne, UK), GeneTex (Irvine, CA, USA), and Vector Laboratories (Burlingame, CA, USA), respectively.

Construction of the 3D gingival tissue culture system. This study was approved by the Ethics Committee of the Nihon University School of Dentistry (#EP19D0011). After obtaining written informed consent, fragments of gingival tissue were obtained from a periodontally healthy patient (a 59-year-old male, non-smoker) during tooth extraction surgery (the left lower third molar) at Nihon University Dental Hospital. Primary gingival fibroblasts were obtained as described previously [24,25]. Briefly, gingival tissues were treated with dispase I (GODO SHUSEI, Tokyo, Japan) and the epithelial layers were separated from the lamina propria and minced lamina propria layers was placed in each well of 6-well plates. Sprouting cells from the lamina propria layers were collected as human primary gingival fibroblasts (hGFBs); I used hGFBs up to the 15^{th} generation [25]. hGFBs and human gingival epithelial Ca9-22 cells, which are frequently used as a

counterpart of gingival epithelial cells [3], were maintained in 10% fetal bovine serum (FBS; Biowest, Nuaillé, France) Minimum Essential Medium α (MEMα; Wako, Osaka, Japan) supplemented with 1% penicillin/streptomycin (Wako). hGFBs suspended in FBS (500 μL, 2.5×10^5 cells/mL) were mixed with 2.3 mL of Cellmatrix type I-A collagen sol (Nitta Gelatin, Osaka, Japan), 760 μL of 5 × Dulbecco's modified Eagle medium (Nitta Gelatin), and 330 μL of reconstitution buffer (Nitta Gelatin, Fig. 7A, panel a). The mixture was placed in a 0.4 μm-pore-size transwell insert (for 12 well plates, Corning, Corning, NY, USA) and incubated for 30 min at 37°C (Fig. 7A, panel b). A Ca9-22 cell suspension (1×10^5 cells/mL, 300 μL) in Epilife medium (Thermo Fisher Scientific, Waltham, MA, USA) containing supplement S7 (Thermo Fisher Scientific) was placed on the gel and incubated overnight at 37°C. MEMα containing 10% FBS was then added to the lower chambers and incubated for a 24 h to form epithelial monolayers on the collagen gels (Fig. 7A, panel c). The epithelial layers were exposed to air by aspiration to induce epithelial stratification (Fig. 7A, panel d). During this step, the medium in the lower chambers was replaced every other day.

Hematoxylin and eosin (HE) staining and immunohistochemistry. Blocks of 3D cultures were fixed in 10% formalin and embedded in paraffin. The blocks were sectioned vertically, and sections were stained with HE. Immunohistochemical triple staining was

performed using an anti-human cytokeratin monoclonal antibody, anti-human vimentin monoclonal antibody, and 4′,6-diamidino-2-phenylindole as a nuclear counterstain.

Stimulation with butyrate in 3D and 2D culture systems. Sodium butyrate (Wako) was diluted in 1% FBS Roswell Park Memorial Institute 1640 (RPMI1640, Wako). Sodium-butyrate-containing media (0, 2.5, 5, 10, 15, and 20 mM butyrate; 600 μL) was added to the upper chamber of the co-cultures (Fig. 7A, panel e). After incubation for 0, 24, 48, and 72 h at 37°C, conditioned media in the upper chambers were collected and centrifuged at 3,000 rpm. Supernatants (550 μL) were collected and used for DNA analysis and western blotting. Ca9-22 cell 2D cultures were also treated with or without 20 mM butyrate. After incubation, collected supernatants were used for DNA analysis.

Measurement of released DNA. Aliquots of cell culture supernatant (100 μL/well) were placed in a 96-well black plate (Greiner Bio-One, Kremsmünster, Austria), and 100 μL/well of 400 nM SYTOX-green dye (Thermo Fisher Scientific) in RPMI1640 was added. Fluorescence intensity (Ex/Em = 485/535 nm) was measured using a Wallac ArvoSX1420 spectrofluorometer (PerkinElmer, Waltham, MA, USA).

Western blot. Aliquots of cell culture supernatant (20 μL/lane) were subjected to western blotting using an anti-Sin3A associated protein SAP130 rabbit polyclonal antibody as the primary antibody and WestVision secondary antibody labeled with horseradish

peroxidase. Clarity Western ECL substrate (Bio-Rad, Hercules, CA, USA) and ChemiDoc XRS (Bio-Rad) were used for visualization.

Statistical analysis. Each experiment was repeated more than twice, and similar results were obtained from each independent experiment. Non-normal distribution of data was determined using the Shapiro-Wilk test. The Kruskal-Wallis test, followed by the Steel test, was used to examine differences. *P*-values < 0.01 were considered statistically significant.

Results

Based on HE-staining data, I detected the construction of a stratified epithelium on collagen gel containing fibroblasts (Fig. 7B). Immunohistochemical staining showed that cytokeratin, an epithelial marker, was present only in the stratified epithelial layer (Fig. 7C, upper left panel). Vimentin, a fibroblast marker, was detected only in the lamina propria layer (Fig. 7C, upper right panel). These findings demonstrated that gingival epithelial cells and fibroblasts did not invade each other (Fig. 7C, lower right panel).

A high butyrate concentration can affect the gingival epithelium at the mature dental plaque that is in close contact with gingival epithelial cells. Thus, I examined the effect of butyrate on the epithelial layers of 3D gingival cultures. Treatment of epithelial layers with butyrate induced DNA release in a time-dependent manner, and the amount of released DNA was significantly higher than that induced by control treatment (Fig. 8A). In addition, butyrate induced DNA release in a dose-dependent manner (Fig. 8B). Furthermore, butyrate induced SAP130 release in a dose-dependent manner (Fig. 8C). To compare the effects of butyrate treatment between 2D and 3D systems, the time-course of DNA release from the 2D culture during butyrate treatment was examined. Treating epithelial layers of the gingival 3D model with butyrate time-dependently increased DNA release until 72 h (Fig. 8A). Although the amount of DNA released from the 2D system

during butyrate treatment increased in a time dependent manner until 48 h (Fig. 8D), it tended to decrease after 48 h (Fig. 8D).

Discussion

In the present study, I developed a 3D gingival culture system consisting of both stratified gingival epithelium and lamina propria layers. As shown in Fig. 7B and C, Ca9-22 cells were not observed in the lamina propria layer of the 3D culture system, and fibroblasts were not detected in epithelial layers. In addition, this system allows gingival epithelial cells to obtain nutrients via the lamina propria. Therefore, this double-layered tissue system is anatomically similar to the actual gingival tissue. However, in my system, I used a gingival epithelial Ca9-22 cell line as a source of gingival epithelial cells. Although the cell line is easy to handle, cell characteristics, such as cell shape and growth speed, occasionally differ from those of primary gingival epithelial cells. I attempted to obtain primary gingival epithelial cells from clinical samples as described previously [24,25], gingival epithelial cells failed to sprout from pieces of clinically obtained gingival epithelium and sometimes dead during maintenance. The condition of the clinically obtained tissues, coverslip placement, passage timing, or other unidentified reasons could underlie these failures. Xiao et al. have developed a similar 3D model. The authors used the immortalized human skin epidermal keratinocyte cell line HaCaT, which reportedly differentiates into stratification layers [26,27]. However, this cell line is aneuploid and not derived from gingival tissue [26]. Although the development of a 3D

culture system using primary gingival epithelial cells is anticipated, a realistic approach for continuous use of a human gingival 3D culture model could be the model developed in the present study or that of Xiao et al.

Similar to previous reports that used 2D gingival culture systems [4], treating the epithelial layer of the 3D culture systems with butyrate could induce release of intracellular molecules such as DNA and SAP130 (Fig. 8). Although butyrate treatment of 3D epithelial layers resulted in an increased release of DNA over time until 72 h (Fig. 8A), the amount of released DNA decreased after 48 h in the 2D model (Fig. 8D). These observations could be attributed to the following reasons: (i) enzymes that the 2D model may release cleave DNA after 48 h, (ii) the 3D model may not release DNA digesting enzymes, and (iii) the 3D culture may release molecules that inhibit DNA digestion.

DAMPs released following butyrate treatment can bind to receptors on surrounding cells and induce the production of proinflammatory cytokines [28]. This indicates that SCFA production from mature dental plaque bacteria may be one of the most important inducers of gingivitis. If molecular mechanisms controlling DAMP release after or during SCFA action can be established, effective methods to suppress periodontal disease can be developed. Therefore, a more complex 3D gingival culture system, which has blood vessels in the lamina propria and so on, is required to evaluate the precise mechanism

underlying the development of gingivitis.

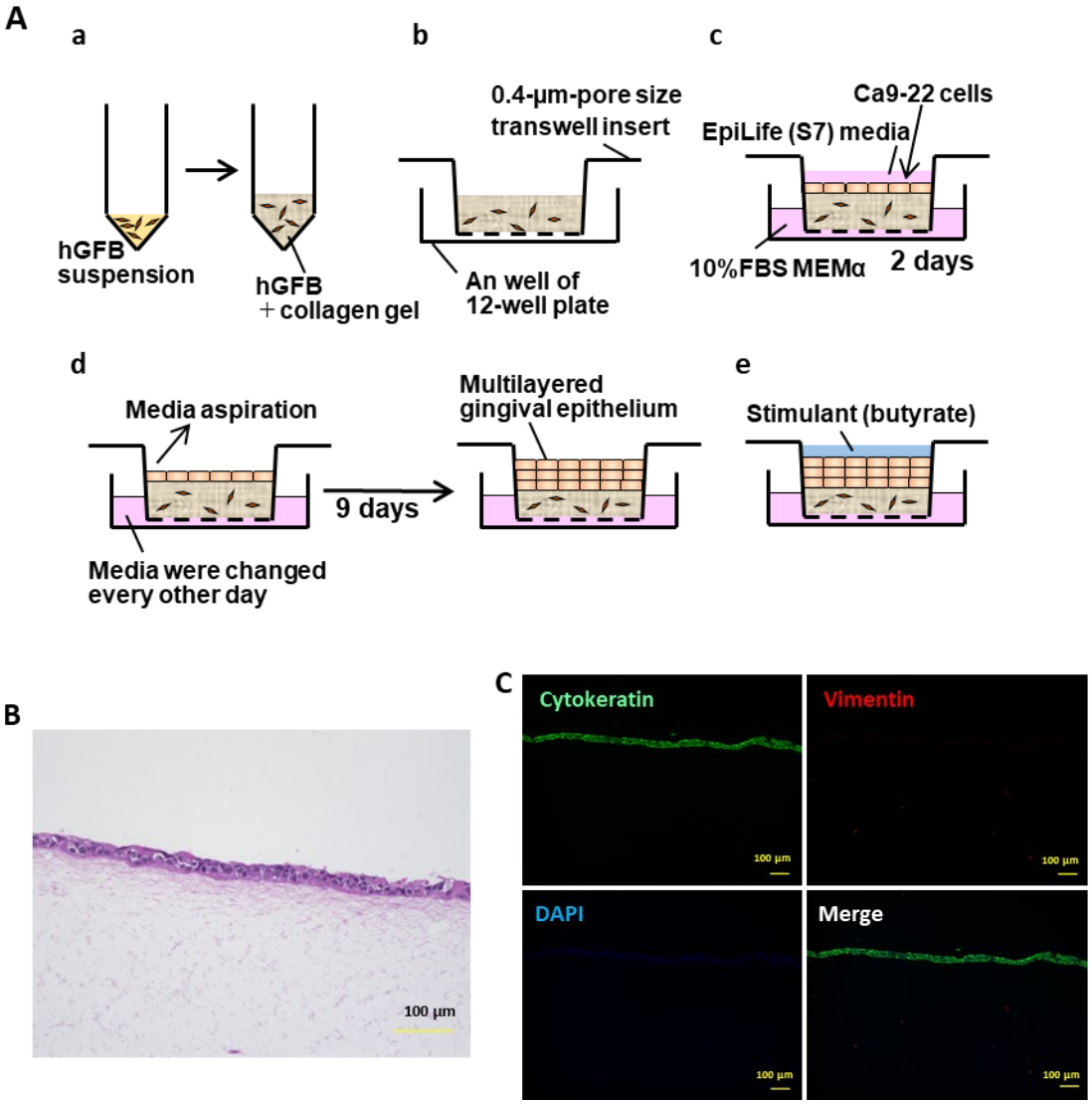

Fig. 7 Construction of a three-dimensional gingival tissue system. (A) Human primary gingival fibroblasts (hGFBs) suspension in collagen sol (a) was poured into transwell inserts (b). After collagen gelation, the Ca9-22 cell suspension was placed on the gel and incubated for 2 days (c). Gingival epithelial monolayers were exposed to the air for 9 days to trigger epithelial stratification (d). The multilayered epithelium was treated with butyrate-containing media (e). (B) The three-dimensional culture was fixed, embedded in paraffin, sectioned, and stained with hematoxylin and eosin. Scale bar: 100 μm. (C) Immunohistochemistry analysis of a representative section. Green: Cytokeratin. Red: Vimentin. Blue: 4′,6-diamidino-2-phenylindole counterstain.

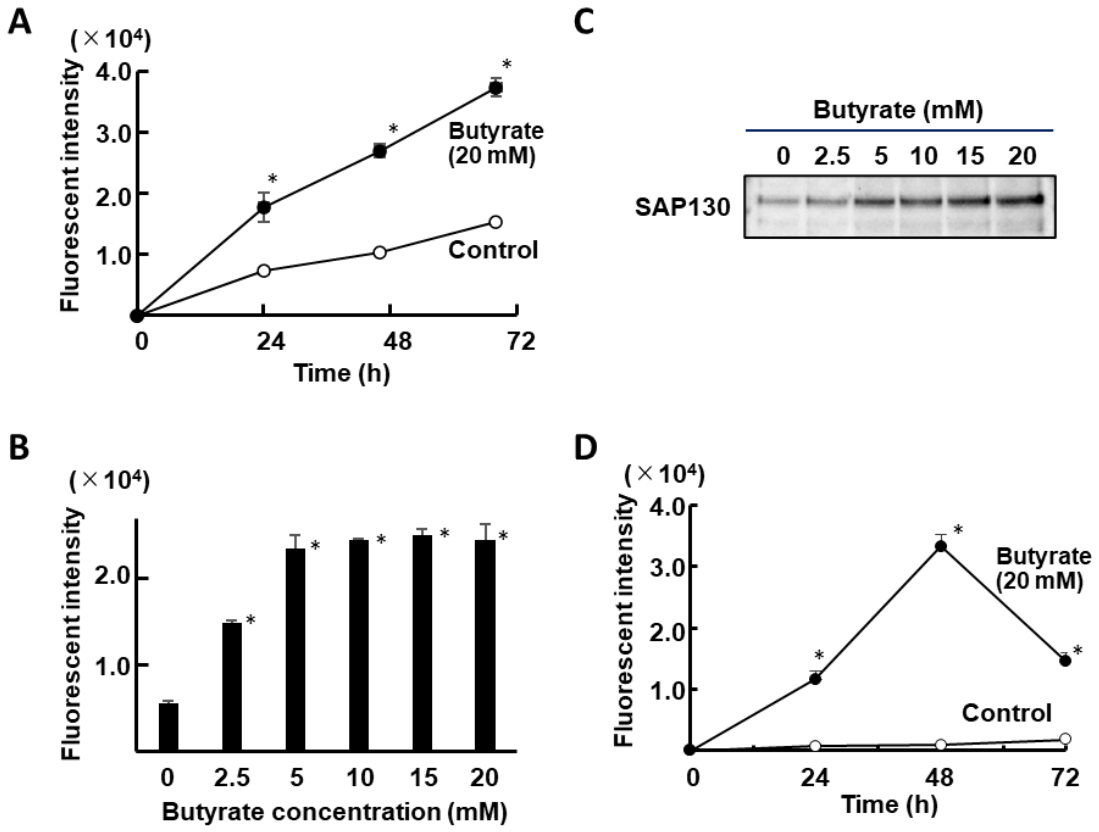

Fig. 8 Butyrate treatment induces the release of cellular components from gingival epithelial layers of the 3D gingival culture system. (A) Time-course of the amount of DNA released during butyrate treatment. The amount of DNA in the conditioned media was measured using SYTOX-green dye (n = 4, *, $P < 0.01$ compared to the control treatment). (B) Butyrate treatment for 72 h induces dose-dependent DNA release from epithelial cells of the 3D gingival culture system (n = 4, *, $P < 0.01$ compared to control treatment). (C) Western blot analysis using conditioned media showed that butyrate treatment for 72 h induced SAP130 release from the epithelial layer of the 3D gingival culture system. (D) Time-course of the amount of DNA released during butyrate treatment of the 2D Ca9-22 cell culture (n = 4, *, $P < 0.01$ compared to control treatment).

Overview

Bacteria in the dental plaque surrounding marginal gingival crevices are thought to cause periodontal disease. Gingival epithelial cells close proximity to mature dental plaque are at risk of exposure to high concentration of SCFAs. SCFA treatment with gingival cells induces cell death, and subsequent release of DAMPs, which evoke inflammation. Therefore, unveiling cell-death induction mechanisms is very important for understanding periodontal diseases, especially for gingivitis. In this study, I examined the mechanisms with focus on HDAC activity of SCFAs. In addition, I developed a 3D gingival tissue model. From these two studies, I demonstrated new findings listed below.

1. Among SCFAs, not only butyrate but also propionate has HDAC inhibitory effect.
2. Induced level of histone acetylation by HDAC inhibitory activities of butyrate and propionate is important for SCFA-induced gingival epithelial Ca9-22 cell death.
3. Genes related to autophagy and ROS generation were upregulated by histone acetylation induced by butyrate treatment.
4. A 3D gingival culture model using primary gingival fibroblast and gingival epithelial Ca9-22 cells was developed.
5. Butyrate stimulation with epithelial side of 3D gingival co-culture system can induce

epithelial cell death and release of DNA and SAP130, a DAMPs, from epithelial layers. Taken together, butyrate and propionate-induced gingival epithelial cell death is epigenetically controlled by HDAC inhibitory effect of SCFAs. In addition, butyrate also induces similar gingival cell death on newly developed 3D-gingival co-culture system.

Acknowledgments

I express my sincere thanks to Prof. Tonogi, Department of Oral and Maxillofacial Surgery I, Nihon University School of Dentistry, for his sophisticated tutelage. I am grateful to Associate Prof. Tsuda, Department of Biochemistry Nihon University School of Dentistry, for his enthusiastic mentorship and his dedicated help. I would like to thank Dr. Mikami (Division of Microscopic Anatomy, Niigata University Graduate School of Medical and Dental Sciences), Dr. Shinozuka (Department of Oral and Maxillofacial Surgery I, Nihon University School of Dentistry), Dr. Yamaguchi (Department of Biochemistry Nihon University School of Dentistry) and Dr. Watanabe (Department of Chemistry Nihon University School of Dentistry) for their helpful suggestions and discussions. I would like to say thanks to Dr. Kirihara, Mr. Kurosawa, and Dr. Yamaguchi for their friendship as a colleague.

Conflict of interest

The author declares no conflict of interest associated with this thesis.

References

1. Pöllänen MT, Salonen JI, Uitto VJ (2003) Structure and function of the tooth-epithelial interface in health and disease. Periodontol 2000 31, 12-31.

2. Tsuda H, Ochiai K, Suzuki N, Otsuka K (2010) Butyrate, a bacterial metabolite, induces apoptosis and autophagic cell death in gingival epithelial cells. J Periodontal Res 45, 626-634.

3. Evans M, Murofushi T, Tsuda H, Mikami Y, Zhao N, Ochiai K et al. (2017) Combined effects of starvation and butyrate on autophagy-dependent gingival epithelial cell death. J Periodontal Res 52, 522-531.

4. Fujiwara Y, Murofushi T, Koshi R, Mikami Y, Tsuda H (2021) Reactive oxygen species-dependent release of damage-associated molecular patterns from human gingival epithelial Ca9-22 cells during butyrate or propionate exposure. J Oral Sci 63, 195-197.

5. Kumar V, Thakur JK, Prasad M (2021) Histone acetylation dynamics regulating plant development and stress responses. Cell Mol Life Sci 78, 4467-4486.

6. Davie JR (2003) Inhibition of histone deacetylase activity by butyrate. J Nutr 133, 2485S-2493S.

7. Hirose K, Isogai E, Mizugai H, Ueda I (1996) Adhesion of Porphyromonas

gingivalis fimbriae to human gingival cell line Ca9-22. Oral Microbiol Immunol 11, 402-406.

8. Ohshima M, Noguchi Y, Ito M, Maeno M, Otsuka K (2001) Hepatocyte growth factor secreted by periodontal ligament and gingival fibroblasts is a major chemoattractant for gingival epithelial cells. J Periodontal Res 36, 377-383.

9. Saito A, Inagaki S, Kimizuka R, Okuda K, Hosaka Y, Nakagawa T et al. (2008) Fusobacterium nucleatum enhances invasion of human gingival epithelial and aortic endothelial cells by Porphyromonas gingivalis. FEMS Immunol Med Microbiol 54, 349-355.

10. Takeuchi H, Setoguchi T, Machigashira M, Kanbara K, Izumi Y (2008) Hydrogen sulfide inhibits cell proliferation and induces cell cycle arrest via an elevated p21 Cip1 level in Ca9-22 cells. J Periodontal Res 43, 90-95.

11. Zhou Y, Zhou B, Pache L, Chang M, Khodabakhshi AH, Tanaseichuk O et al. (2019) Metascape provides a biologist-oriented resource for the analysis of systems-level datasets. Nat Commun 10, 1523.

12. Kanda Y (2013) Investigation of the freely available easy-to-use software 'EZR' for medical statistics. Bone Marrow Transplant 48, 452-458.

13. Chauhan S, Mandell MA, Deretic V (2015) IRGM governs the core autophagy

machinery to conduct antimicrobial defense. Mol Cell 58, 507-521.

14. Maruyama T, Noda NN (2018) Autophagy-regulating protease Atg4: structure, function, regulation and inhibition. J Antibiot (Tokyo), 71, 72-78.

15. Kotani T, Kirisako H, Koizumi M, Ohsumi Y, Nakatogawa H (2018) The Atg2-Atg18 complex tethers pre-autophagosomal membranes to the endoplasmic reticulum for autophagosome formation. Proc Natl Acad Sci U S A 115, 10363-10368.

16. Fulton DJ (2009) Nox5 and the regulation of cellular function. Antioxid Redox Signal 11, 2443-2452.

17. Ebe N, Hara-Yokoyama M, Iwasaki K, Iseki S, Okuhara S, Podyma-Inoue KA et al. (2011) Pocket epithelium in the pathological setting for HMGB1 release. J Dent Res 90, 235-240.

18. Kim J, Kundu M, Viollet B, Guan KL (2011) AMPK and mTOR regulate autophagy through direct phosphorylation of Ulk1. Nat Cell Biol 13, 132-141.

19. Azad MB, Chen Y, Gibson SB (2009) Regulation of autophagy by reactive oxygen species (ROS): implications for cancer progression and treatment. Antioxid Redox Signal 11, 777-790.

20. Liu J, Wang Y, Meng H, Yu J, Lu H, Li W et al. (2019) Butyrate rather than LPS

subverts gingival epithelial homeostasis by downregulation of intercellular junctions and triggering pyroptosis. J Clin Periodontol 46, 894-907.

21. Berthelot F, Fattoum L, Casulli S, Gozlan J, Marechal V, Elbim C (2012) The effect of HMGB1, a damage-associated molecular pattern molecule, on polymorphonuclear neutrophil migration depends on its concentration. J Innate Immun 4, 41-58.

22. Huang W, Tang Y, Li L (2010) HMGB1, a potent proinflammatory cytokine in sepsis. Cytokine 51, 119-126.

23. Antoni D, Burckel H, Josset E, Noel G (2015) Three-dimensional cell culture: a breakthrough in vivo. Int J Mol Sci 16, 5517-5527.

24. Ohshima M, Yamaguchi Y, Matsumoto N, Micke P, Takenouchi Y, Nishida T et al. (2010) TGF-beta signaling in gingival fibroblast-epithelial interaction. J Dent Res 89, 1315-1321.

25. Yamaguchi Y, Saito A, Horie M, Aoki A, Micke P, Ohshima M et al. (2021) Targeting hepatocyte growth factor in epithelial-stromal interactions in an in vitro experimental model of human periodontitis. Odontology 109, 912-920.

26. Boukamp P, Petrussevska RT, Breitkreutz D, Hornung J, Markham A, Fusenig NE (1988) Normal keratinization in a spontaneously immortalized aneuploid human

keratinocyte cell line. J Cell Biol 106, 761-771.

27. Xiao L, Okamura H, Kumazawa Y (2018) Three-dimensional inflammatory human tissue equivalents of gingiva. J Vis Exp. doi: 10.3791/57157.

28. Gong T, Liu L, Jiang W, Zhou R (2020) DAMP-sensing receptors in sterile inflammation and inflammatory diseases. Nat Rev Immunol 20, 95-112.

Articles composing this thesis

This thesis is composed by two articles listed below.

1. Kazuki Uemichi, Yoshikazu Mikami, Takayasu Watanabe, Keiji Shinozuka, Morio Tonogi, and Hiromasa Tsuda. Histone-deacetylase-inhibitory effects of periodontopathic-bacterial metabolites induce human gingival epithelial Ca9-22 cell death. ***Odontology, Epub ahead of press*** (https://doi.org/10.1007/s10266-022-00775-9).

2. Yusuke Kurosawa, Hirofumi Yamaguchi, Kazuki Uemichi, Keiji Shinozuka, Yuki Kirihara, and Hiromasa Tsuda. Butyrate-treatment induces gingival epithelial cell death in a three-dimensional gingival-connective tissue hybrid co-culture system. ***J Dent Sci, Epub ahead of press*** **(**https://doi.org/10.1016/j.jds.2022.08.034).